

## Electronic band structure of pentacene: An experimental and theoretical study

S. Berkebile,<sup>1,\*</sup> P. Puschnig,<sup>2</sup> G. Koller,<sup>1</sup> M. Oehzelt,<sup>1,†</sup> F. P. Netzer,<sup>1</sup> C. Ambrosch-Draxl,<sup>2</sup> and M. G. Ramsey<sup>1,‡</sup>

<sup>1</sup>*Institute of Physics, Surface and Interface Physics, Karl-Franzens University, A-8010 Graz, Austria*

<sup>2</sup>*Chair of Atomistic Modelling and Design of Materials, University of Leoben, A-8700 Leoben, Austria*

(Received 15 November 2007; published 11 March 2008)

The intermolecular and intramolecular dispersions of pentacene are measured by angle resolved photoemission spectroscopy using a uniaxially aligned crystalline thin film. The band structure perpendicular to the molecules displays a small dispersion in agreement with density functional theory (DFT). Parallel to the molecules, two  $\pi$  bands consisting of five and six orbitals are clearly observed. In these intramolecular bands, the orbital emissions are shown to be in agreement with calculations of the photoemission intensities based on DFT both in terms of position and width in momentum space.

DOI: [10.1103/PhysRevB.77.115312](https://doi.org/10.1103/PhysRevB.77.115312)

PACS number(s): 79.60.Fr, 71.15.Mb, 71.20.Rv, 73.20.At

### INTRODUCTION

Pentacene (5A) is a prototypical  $\pi$ -conjugated organic molecule, the optoelectronic properties of which are presently attracting interest from both the applied and basic science communities. Recently, basic studies have focused on the electronic-vibrational coupling,<sup>1,2</sup> molecular orientation,<sup>3,4</sup> crystal structure,<sup>5–8</sup> and electronic structure<sup>9–13</sup> of 5A. The complete valence band of 5A has been little explored as angle-resolved ultraviolet photoemission spectroscopy (ARUPS) studies of the electronic structure have concentrated on the highest occupied molecular orbital (HOMO), where surprisingly high intermolecular dispersion has been observed.<sup>11,13</sup> Attempts made in the literature to identify further UPS orbital emissions<sup>3,4</sup> have been hampered by the overlap in energy between the molecular emission peaks of all orbitals except the HOMO. To obtain an unambiguous assignment of the UPS orbital emissions and the band structure require highly ordered samples, allowing the exploitation of not only the energies of the molecular orbitals but also their particular symmetries, as momentum is equivalent to a symmetry assignment.<sup>14</sup>

The ability to control the growth of thin organic films with crystallites of a single orientation or with symmetry equivalent domains in experimentally accessible geometries has been demonstrated only in recent years.<sup>15–17</sup> Using ARUPS to measure such a system in which all molecules have the same orientation enables the energy and momentum of the individual orbitals and their spread to be accurately determined, as has been recently accomplished for the  $\pi$  bands of *para*-sexiphenyl.<sup>18</sup> For such measurements of *intramolecular* dispersion, it is essential to obtain films of uniaxially aligned molecules and to keep the amount of disorder to a minimum. This alignment is achieved here by the use of a substrate with anisotropic template properties which aligns the molecules parallel to a substrate azimuth. Previous measurements of phenyl and alkyl chains have demonstrated an angular photoemission behavior that is indicative of intramolecular dispersion but have been unable to distinguish individual molecular orbitals.<sup>19–22</sup>

Here we present band structure measurements,  $E$  vs  $k$ , of the entire  $\pi$  orbital region in directions both parallel and perpendicular to the long molecular axis obtained from high-

quality crystalline films of uniaxially oriented pentacene [5A(022)]. Parallel to the molecules the energy-momentum relationship observed is that of the individual molecules, i.e., the intramolecular band structure. The positions and  $k$  widths of the orbitals of the two  $\pi$  bands observed are shown to be in agreement with density functional theory calculations for the isolated 5A molecule. In contrast, the dispersion found perpendicular to the molecules reflects the crystal periodicity with the experimental intermolecular band structure in good agreement with the calculated band dispersion.

### EXPERIMENTAL AND THEORETICAL

5A(022) films were grown and measured *in situ* in ultra-high vacuum on the  $p(2 \times 1)$  oxygen reconstructed Cu(110) substrate template surface.<sup>23</sup> Pentacene (Fluka) was deposited *in situ* using a nominal growth rate of  $4 \text{ \AA min}^{-1}$ . After a deposition of  $200 \text{ \AA}$  5A on the Cu(110)- $p(2 \times 1)$ O surface at 100 K, the film was brought to 300 K overnight. This procedure was used to control the morphology in order to avoid a superposition of the multilayer features with substrate and monolayer features, which are difficult to suppress in films grown at room temperature due to the propensity of 5A to island. Near-edge x-ray absorption spectroscopy and x-ray diffraction (XRD) show that the long axis of the molecules in such films are parallel to the [001] substrate direction, with the 5A(022) crystallite orientation of the structure reported in Mattheus *et al.*,<sup>5</sup> as depicted in Fig. 1.

In the photoemission experiment, only the momentum component of the outgoing photoelectron parallel to the surface  $k_{\parallel}$  is conserved. The electronic structure parallel to the surface  $E(k_{\parallel})$  can be determined by measuring the photoemission spectrum as a function of photoelectron emission angle  $\theta$  at constant photon energy. The relation between  $\theta$  and  $k_{\parallel}$  is given by

$$k_{\parallel} = \sqrt{2m_e E_{\text{kin}} / \hbar^2} \sin \theta. \quad (1)$$

ARUPS was performed in a VG ADES 400 spectrometer using unpolarized helium I radiation ( $h\nu=21.2 \text{ eV}$ , photon incidence angle of  $\alpha=60^\circ$ ) and an electron energy analyzer on a single axis goniometer in the specular plane with an angular resolution of  $\pm 1^\circ$  ( $\Delta k_{\text{max}} < 0.08 \text{ \AA}^{-1}$ ). Total energy

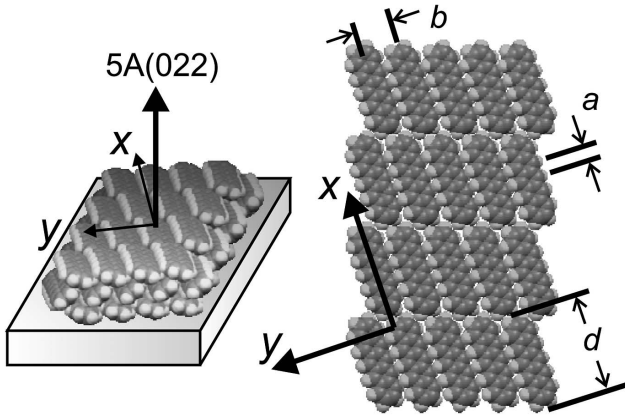


FIG. 1. A model of 5A(022) bulk termination (left) and the top view (right). Interlayer spacing  $a=2.35$  Å, interplane spacing  $d=14.77$  Å, and lateral spacing  $b=6.41$  Å are indicated.

resolution was  $\sim 80$  meV at 300 K as determined by the Cu(110)-(2 $\times$ 1)O Fermi edge.

All calculations are based on a first-principles density functional approach and have been performed with the ABINIT package, a plane-wave based implementation of density functional theory for periodic systems.<sup>24</sup> The photoemission intensities have been calculated for an isolated 5A molecule using a supercell approach with a box size of  $63.5 \times 10.6 \times 10.6$  Å<sup>3</sup>.

The angular dependent photoelectron emission intensity is given by Fermi golden rule.<sup>25</sup> By approximating the final state by a plane wave, an approach which neglects photoelectron diffraction effects of the outgoing wave, one can write the photoemission intensity in the dipole approximation as

$$I(\hat{r}, \mathbf{k}_f) = \frac{2\pi}{\hbar} |\langle e^{-i\mathbf{k}_f \cdot \mathbf{r}} | \mathbf{p} \cdot \mathbf{A} | \psi_{n\mathbf{k}_i} \rangle|^2 \delta(E_{f,\text{kin}} - E_i - \hbar\omega), \quad (2)$$

summing over all transitions from occupied initial states  $n\mathbf{k}_i$  described by Bloch wave functions  $\psi_{n\mathbf{k}_i}$  to a plane-wave final state  $e^{-i\mathbf{k}_f \cdot \mathbf{r}}$ , where  $\mathbf{p}$  denotes the momentum operator and  $\mathbf{A}$  the vector potential of the exciting electromagnetic wave. The  $\delta$  function assures energy conservation. In a plane-wave pseudopotential approach, the initial state wave function  $\psi_{n\mathbf{k}_i}(\mathbf{r})$  is expanded into plane waves, and, thus, the intensity can be written as

$$I \propto |(\mathbf{k}_f \cdot \mathbf{A}) \tilde{u}_{n\mathbf{k}_i}(\mathbf{G})|^2, \quad (3)$$

where  $\tilde{u}_{n\mathbf{k}_i}(\mathbf{G})$  is the Fourier coefficient of the lattice periodic part of the wave function at wave vector  $\mathbf{k}_i$  and band number  $n$ . The term  $\mathbf{k}_f \cdot \mathbf{A}$  adds a smoothly varying prefactor which depends on the angle of incident light  $\alpha$  and the detection angle  $\theta$ . Therefore, the transition matrix elements in Eq. (3) are proportional to the square of the Fourier coefficients of the initial state wave function, and the Fourier transform (FT) of the Kohn-Sham orbitals should be directly related to the photoemission intensity.

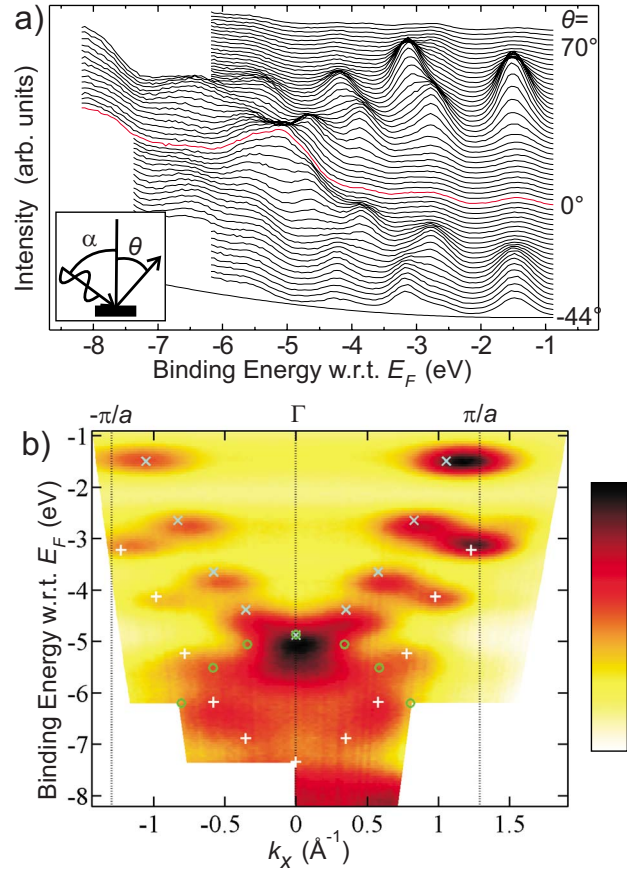


FIG. 2. (Color online) ARUPS measurements along the 5A molecular axis ( $x$  axis in Fig. 1). In (a), spectra from  $\theta=-44^\circ$  to  $+70^\circ$  in  $2^\circ$  steps are shown. The inset indicates the experimental geometry. Spectra in  $1^\circ$  steps are displayed as an  $E(k)$  map in (b) after conversion from  $\theta$  to  $k_x$  by Eq. (1) and after the quadratic curve at the bottom of (a) was subtracted from the data. The Brillouin zone boundaries of a hypothetical infinitely long acene ( $\pi/a=2.35$  Å<sup>-1</sup>) are indicated. The color scale (gray scale) represents an arbitrary linear intensity scale. Calculations for an isolated molecule are represented by symbols which have been rigidly shifted to agree with the measured HOMO energy: upper ( $\times$ ) and lower ( $+$ )  $\pi$  bands and first  $\sigma$  band ( $\circ$ ).

## RESULTS AND DISCUSSION

Valence band photoemission spectra were measured along the molecular axis in the (022) 5A plane ( $x$  axis in Fig. 1). In Fig. 2(a), the measured spectra depend greatly on experimental geometry, indicative of the high degree of order of the film. The HOMO orbital emission is clearly visible at a binding energy of  $E_B=-1.5$  eV below the Fermi level ( $E_F$ ) (Ref. 27) and appears strongest at  $\theta=\pm 35^\circ$ . By displaying the photoemission spectra data as an intensity map of  $E(k_x)$  in Fig. 2(b), the angular intensity behavior of the molecular orbitals can be more easily visualized and understood. It is noteworthy that the crystal periodicity of  $\pi/d=0.19$  Å<sup>-1</sup> is not reflected in the data. Unlike measurements perpendicular to the molecules (see later), the molecular orbitals are not observed as continuous bands in  $k_x$  but rather appear over discrete ranges of momentum. Moreover, within the  $k$  ranges

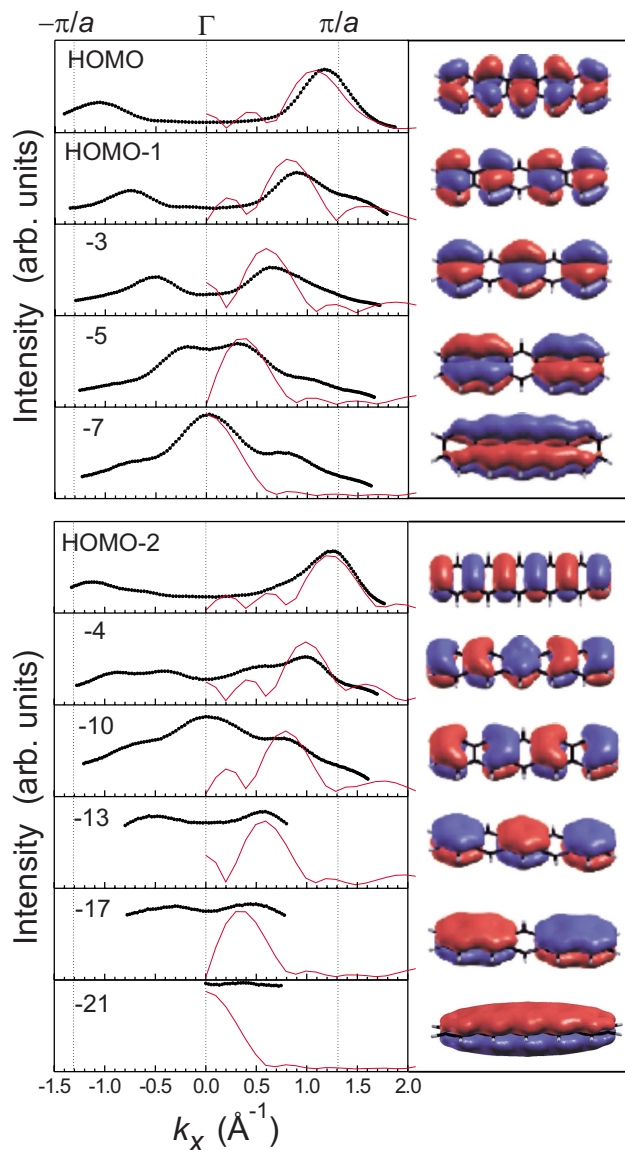


FIG. 3. (Color online) Constant energy line scans of the photoemission intensity map of Fig. 2(b) at 5A  $\pi$  orbital energies. Next to each line scan, the Kohn-Sham orbitals are shown. The Fourier transform of each orbital is displayed as a solid red line (solid gray line) with the experimental data (solid black circles). The binding energies of the line scans are  $-1.53$ ,  $-2.78$ ,  $-3.88$ ,  $-4.68$ ,  $-5.13$ ,  $-3.13$ ,  $-4.18$ ,  $-5.48$ ,  $-6.38$ ,  $-6.88$ , and  $-7.63$  eV from top to bottom. All experimental intensities have the same scale, and the calculations have been scaled so that the HOMO intensities match.

where the orbitals are observed no energy dispersion is apparent. The emissions are comprised of two distinct sets of molecular orbitals which are symmetric around the  $\Gamma$  point ( $\theta=0^\circ$ ). These sets are referred to as the upper and lower molecular “ $\pi$  bands.” The upper  $\pi$  band contains five orbitals starting at the  $\Gamma$  point at  $E_B=-5.2$  eV and running up to the HOMO with a peak position at  $k_x=1.18 \text{ \AA}^{-1}$  and  $E_B=-1.5$  eV.

The energy and momentum of the orbitals of these two bands are in agreement with calculations for an isolated 5A molecule. The symbols in Fig. 2 indicate the momentum po-

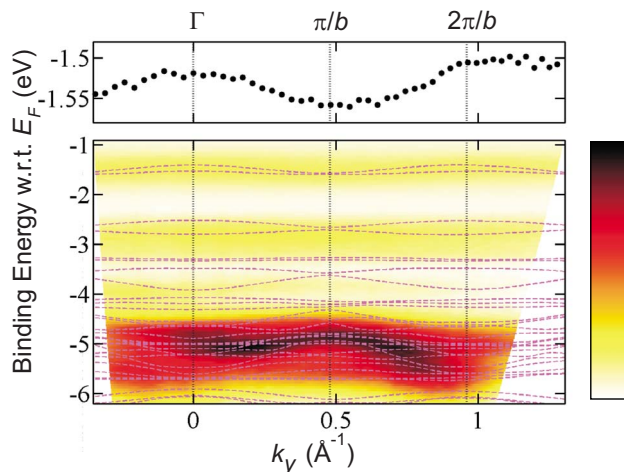


FIG. 4. (Color online) ARUPS measurements perpendicular to the 5A molecular axes ( $y$  axis in Fig. 1). Spectra from  $\theta=-10^\circ$  to  $+40^\circ$  in  $1^\circ$  steps are displayed as an  $E(k)$  map after conversion from  $\theta$  to  $k_y$  by Eq. (1) and subtraction of a quadratic curve to simulate the secondary electron background. The Brillouin zone boundaries of the 5A crystal ( $\pi/b=0.49 \text{ \AA}^{-1}$ ) are indicated. The color scale (gray scale) represents an arbitrary intensity scale. The top panel shows the center of a Gaussian peak fit of the HOMO emissions. Theoretical calculations in the corresponding crystal direction are shown by purple (gray) dashed lines.

sition of the largest peak in the FT of each orbital of the isolated molecule at the corresponding calculated orbital energy. Calculations place the three lower orbitals of the lower  $\pi$  band and several  $\sigma$  orbitals in the area of large emission density below a binding energy of  $-5$  eV where it becomes difficult to identify individual peaks. The photoemission intensity versus momentum at the energy corresponding to each  $\pi$  orbital is shown in Fig. 3 in conjunction with their FTs. As is evident in the figure, the positions and widths in  $k_x$  are well reproduced by the calculations.

The behavior of the  $\pi$  orbitals in  $E(k_x)$  can be interpreted in terms of band structure, familiar for infinite systems. In this finite system of 22 carbon atoms, 11 fully occupied  $p_z$ -derived orbitals give rise to two molecular  $\pi$  bands: five orbitals from the pairs of apex carbons and six from the linking and end carbon pairs. These basis orbitals can easily be identified in the highest orbital of each  $\pi$  band, the HOMO and HOMO-2 of Fig. 3.

Once the nature of these two bands is understood, a couple of interesting points can be made by a comparison of the 5A intramolecular band structure to that of the hypothetical infinite acene polymer. The most obvious differences is that the limited number of units leads to the limited number of orbitals, rather than a continuous band of infinite number,<sup>14</sup> and there is a different number of orbitals in each band. A further consequence of the limited number of units is that the momentum of these orbitals is spread. An orbital derived from a chain with an infinite number of units will be infinitely sharp in momentum. In the finite molecule, the perfect translational symmetry is broken and the Bloch vector must be replaced by a distribution in  $k$  space inversely proportional to the length over which there is some period-



icity. Alternatively, to obtain zero electron density outside of the molecule requires more than one Bloch vector, leading to a spread in momentum. These arguments in terms of Fourier components of a spatially confined wave function are equivalent to the structure factor arguments of Narioka *et al.*<sup>20</sup> Moreover, the highest orbital of each 5A  $\pi$  band deviates from the Brillouin zone boundary (BZB) expected for an infinite polymer at  $\pi/a$ . This deviation is most easily recognized in the HOMO, which is strongly affected by the finite chain length. The wave function maxima of the HOMO are not centered on the apex atom position and their spacings are slightly larger than the ring periodicity  $a$ , causing the weight of the Fourier components to move in toward  $\Gamma$  from the polymer BZB.<sup>28</sup> This deviation is less pronounced in the HOMO-2, where, as can be seen in Fig. 3, the wave function maxima reside at positions closer to the ring periodicity, resulting in a HOMO-2 orbital emission closer to  $\pi/a$ . It should be noted that the observation of intramolecular band dispersion indicates no significant orbital overlap in the direction of the molecular axes, similar to that recently observed in sexiphenyl (6P).<sup>18</sup> Unlike 6P, both 5A  $\pi$ -bands disperse in the same direction have highest intensity in the first Brillouin zone and have different numbers of orbitals in the two bands with, as discussed earlier, the  $k$  position in one band deviating significantly from that of the isolated molecule.

The band map measured perpendicular to the molecular axis [ $E(k_y)$ ] is displayed in Fig. 4. In this direction, bands of continuous intensity over the full range of momentum are observed. On close inspection, periodic variations in energy can be seen with turning points at  $\pi/b$  corresponding to the BZB of the 5A crystal, as is clear in the complex region

around  $-5$  eV and also in the mild dispersion of the HOMO-derived band shown in the inset. As can be seen in Fig. 4, the observed band structure is in agreement with that calculated for bulk 5A. Of note is that unlike previously reported results for the HOMO, the average dispersion is in accord with the theory both in magnitude and direction. It is suggested that previous results displaying surprisingly large dispersion may derive from different 5A polymorphs, for example, the 5A thin film phase, where a much larger energy separation between the two HOMO bands has been predicted.

## CONCLUSIONS

Here, the band structure of the entire  $\pi$  band of pentacene has been experimentally determined and shown to be in accord with *ab initio* calculations. The results highlight the importance of controlling the crystallinity and morphology of organic films for unambiguous results. Measurements parallel to the molecules reflect the intramolecular band dispersion whose details are prototypical and significant for understanding acene related systems of finite size and dimensionality. Perpendicular to the molecular axes, continuous bands reflecting the crystal periodicity are observed. Of significance to the ongoing debate on charge transport in pentacene films is the relatively small extent of the dispersion of the HOMO determined both experimentally and theoretically.

## ACKNOWLEDGMENTS

We wish to thank Roland Resel and co-workers for XRD characterization and Egbert Zojer for discussions. This work was funded by the Austrian Science Funds (FWF).

\*stephen.berkebile@uni-graz.at

<sup>†</sup>Present address: Institute of Experimental Physics, Johannes Kepler University Linz, Austria.

<sup>‡</sup>michael.ramsey@uni-graz.at; <http://surface-scienceuni-graz.at>

<sup>1</sup>V. Coropceanu, M. Malagoli, D. A. da Silva Filho, N. E. Gruhn, T. G. Bill, and J. L. Brédas, *Phys. Rev. Lett.* **89**, 275503 (2002).

<sup>2</sup>H. Yamane, S. Nagamatsu, H. Fukagawa, S. Kera, R. Friedlein, K. K. Okudaira, and N. Ueno, *Phys. Rev. B* **72**, 153412 (2005).

<sup>3</sup>H. Ozaki, *J. Chem. Phys.* **113**, 6361 (2000).

<sup>4</sup>P. G. Schroeder, C. B. France, J. B. Park, and B. A. Parkinson, *J. Appl. Phys.* **91**, 3010 (2002).

<sup>5</sup>C. C. Mattheus, A. B. Dros, J. Baas, A. Meetsma, J. L. d. Boer, and T. T. M. Palstra, *Acta Crystallogr., Sect. C: Cryst. Struct. Commun.* **57**, 939 (2001).

<sup>6</sup>R. G. della Valle, E. Venuti, A. Brillante, and A. Girlando, *J. Chem. Phys.* **118**, 807 (2003).

<sup>7</sup>M. Oehzelt, R. Resel, C. Suess, R. Friedlein, and W. R. Salaneck, *J. Chem. Phys.* **124**, 054711 (2006).

<sup>8</sup>A. C. Mayer, A. Kazimirov, and G. G. Malliaras, *Phys. Rev. Lett.* **97**, 105503 (2006).

<sup>9</sup>M. L. Tiago, J. E. Northrup, and S. G. Louie, *Phys. Rev. B* **67**, 115212 (2003).

<sup>10</sup>K. Hummer and C. Ambrosch-Draxl, *Phys. Rev. B* **72**, 205205

(2005).

<sup>11</sup>N. Koch, A. Vollmer, I. Salzmann, B. Nickel, H. Weiss, and J. P. Rabe, *Phys. Rev. Lett.* **96**, 156803 (2006).

<sup>12</sup>H. Fukagawa, H. Yamane, T. Kataoka, S. Kera, M. Nakamura, K. Kudo, and N. Ueno, *Phys. Rev. B* **73**, 245310 (2006).

<sup>13</sup>H. Kakuta, T. Hirahara, I. Matsuda, T. Nagao, S. Hasegawa, N. Ueno, and K. Sakamoto, *Phys. Rev. Lett.* **98**, 247601 (2007).

<sup>14</sup>R. Hoffmann, *Solids and Surfaces: A Chemist's View of Bonding in Extended Structures* (Wiley-VCH, New York, 1988).

<sup>15</sup>G. Koller, S. Berkebile, J. Krenn, G. Tzvetkov, G. Hlawacek, O. Lengyel, F. P. Netzer, C. Teichert, R. Resel, and M. G. Ramsey, *Adv. Mass Spectrom.* **16**, 2159 (2004).

<sup>16</sup>S. Berkebile, G. Koller, G. Hlawacek, C. Teichert, F. P. Netzer, and M. G. Ramsey, *Surf. Sci.* **600**, L313 (2006).

<sup>17</sup>J. Ivanco, T. Haber, J. R. Krenn, F. P. Netzer, R. Resel, and M. G. Ramsey, *Surf. Sci.* **601**, 178 (2007).

<sup>18</sup>G. Koller, S. Berkebile, M. Oehzelt, P. Puschnig, C. Ambrosch-Draxl, F. P. Netzer, and M. G. Ramsey, *Science* **317**, 351 (2007).

<sup>19</sup>K. Seki, U. Karlsson, R. Engelhardt, and E. E. Koch, *Chem. Phys. Lett.* **103**, 343 (1984).

<sup>20</sup>S. Narioka, H. Ishii, K. Edamatsu, K. Kamiya, S. Hasegawa, T. Ohta, N. Ueno, and K. Seki, *Phys. Rev. B* **52**, 2362 (1995).

- <sup>21</sup>D. Yoshimura, H. Ishii, Y. Ouchi, E. Ito, T. Miyamae, S. Hasegawa, K. K. Okudaira, N. Ueno, and K. Seki, *Phys. Rev. B* **60**, 9046 (1999).
- <sup>22</sup>T. Miyamae, S. Hasegawa, D. Yoshimura, H. Ishii, N. Ueno, and K. Seki, *J. Chem. Phys.* **112**, 3333 (2000).
- <sup>23</sup>M. Oehzelt, L. Grill, S. Berkebile, G. Koller, F. P. Netzer, and M. G. Ramsey, *ChemPhysChem* **8**, 1707 (2007).
- <sup>24</sup>X. Gonze *et al.*, *Comput. Mater. Sci.* **25**, 478 (2002).
- <sup>25</sup>P. J. Feibelman and D. E. Eastman, *Phys. Rev. B* **10**, 4932 (1974).
- <sup>26</sup>G. Koller, R. I. R. Blyth, S. A. Sardar, F. P. Netzer, and M. G. Ramsey, *Appl. Phys. Lett.* **76**, 927 (2000).
- <sup>27</sup>The position of the HOMO emission peak with respect to  $E_F$  is dependent on the interaction of the molecular monolayer with the substrate (Ref. 26). A substrate independent ionization potential (IP), referenced to the vacuum level, is obtained by adding the energy position  $E_B$  of the HOMO peak to the work function of the film. Here, IP=6.0 eV.
- <sup>28</sup>The agreement between experiment and theory is better for the linking and end carbon derived band than for the apex carbon derived band and suggests that the isolated molecular orbitals of the apex band are modified in the crystal. Indeed, calculations show that the orbitals of the apex band, which includes the HOMO, have the greatest dispersion and, hence, overlap in the crystal (Ref. 10).